Title

Theoretical Investigation on One-Electron ϕ⋯ϕ Bonding in Diuranium Inverse Sandwich U2B6 Complex Enabled by a B6 Ring.

Journal

Inorganic Chemistry, 63(39)

Authors

Burkhardt, Jordan
Li, Wan-Lu

Publication Date

2024-09-30

DOI

10.1021/acs.inorgchem.4c03446

Inorganic Chemistry

pubs.acs.org/IC

Article

Theoretical Investigation on One-Electron $\phi \cdots \phi$ Bonding in Diuranium Inverse Sandwich U_2B_6 Complex Enabled by a B_6 Ring

Jordan Burkhardt and Wan-Lu Li*

Cite This: *Inorg. Chem.* 2024, 63, 18313−18322

Read Online

ACCESS | Metrics & More | Article Recommendations | Supporting Information

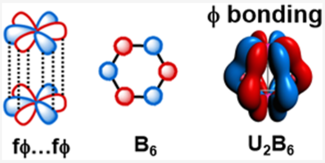

ABSTRACT: Traditional σ, π, and δ types of covalent chemical bonding have been extensively studied for nearly a century. In contrast, ϕ-type bonding involving nf ($n = 4, 5$) orbitals has received less attention due to their high contraction and minimal orbital overlap. Herein, we theoretically predict a singly occupied $\phi \cdots \phi$ bonding between two 5f orbitals, facilitated by B_6 group orbitals in the hexa-boron diuranium inverse sandwich structure of U_2B_6. From *ab initio* quantum chemical calculations, the global minimum structure has a septuplet state with D_{6h} symmetry. Chemical bonding analyses reveal that the 5f and 6d atomic orbitals of the two uranium atoms interact with the ligand orbitals of the central B_6 ring, exhibiting favorable energy matching and symmetry compatibility to form delocalized σ-, π-, δ-, and ϕ-type bonding orbitals. Notably, even though the $\phi \cdots \phi$ bonding orbital is singly occupied, it still has a significant role in stability and cannot be overlooked. Furthermore, the U_2B_6 cluster model can be viewed as a building block of UB_2 solid materials from both geometric and electronic perspectives. This work predicts the first example of $\phi \cdots \phi$ bonding, highlighting the complexity and diversity of chemical bonds formed in actinide boride clusters.

1. INTRODUCTION

The concept of the chemical bond is a fundamental cornerstone of modern chemical science.[1−3] In 1931, Mulliken and Urey established the connection between spectroscopic symbolism and notation for various chemical bonds.[4−6] Since then, covalent chemical bonds in linear molecules can be categorized based on their symmetry and the number of nodal planes along the internuclear axis, including σ, π, δ, and ϕ bonds, which correspond to angular momentum $\Lambda = 0, \pm 1, \pm 2$, and ± 3, respectively.[6,7] Among these, σ bonds, formed by head-on overlapping of orbitals, are generally stronger than π and δ bonds, commonly observed in compounds with multiple bonds.[8−14] In organic and main-group inorganic chemistry, σ and π bonds are ubiquitous, while δ bonding was first identified in 1965 by Cotton as part of the rhenium−rhenium quadruple bond in $[Re_2Cl_8]^{2-}$.[15]

In 1981, Bursten and Ozin proposed the existence of ϕ-type bonding between 5f orbitals in the U_2 molecule, but multireference *ab initio* calculations later revealed this to be antiferromagnetic coupling rather than true ϕ bonding due to minimal overlap of the contracted 5f orbitals.[16,17] Since only 5f orbitals can potentially form ϕ bonding interactions, locating such bonds has been a significant challenge in chemical bonding theory.

Actinide−ligand interactions provide fertile ground for exploring novel bonding features. In Cp-supported uranium metallacyclocumulene complexes, potential ϕ-type interactions have been suggested through side-to-side interactions between U ($5f^1$) and Cp ligands.[18,19] The $U(C_8H_8)_2$ sandwich complex has also shown subtle ϕ bonding interactions via side-to-head patterns.[20] Recent studies have reported head-to-head ϕ back-bonding from uranium f-orbitals into allyl π^* orbitals in allyl uranium sandwich complexes.[21] Despite these advances, direct $\phi \cdots \phi$ bonding in diactinide compounds remains elusive.

Inverse sandwich complexes with aromatic central rings connected to two metals often exhibit diverse delocalized bonds between the metals and the central ring.[22−30] In most of these complexes, ring-coupled σ- and π-type bonding arises from the matching energy levels between the group orbitals of the central ring and the metal orbitals. The diffuse spatial distribution of the metal orbitals allows them to interact with zero- and one-node ring orbitals, forming delocalized σ- and π-bonds, respectively. Cummins and co-workers identified a special δ bond critical for the stability of diuranium inverse sandwich complexes.[31,32] Dilanthanide (Ln) inverse sandwich complexes, such as Ln_2B_8, have been reported to exhibit δ bonds formed by 5d δ and two-node antibonding π orbitals of the B_8 ring, enhancing $Ln-B_8-Ln$ interactions.[33] Inspired by these findings, we hypothesized that $\phi \cdots \phi$ bonding could be facilitated in diactinide inverse sandwich structures by the appropriate ligand orbitals in the central ring.

Here, we present a quantum chemical study of unique one-electron $\phi \cdots \phi$ bonding mediated by delocalized orbitals of a B_6 central ring in a diuranium inverse sandwich complex, U_2B_6. Using both density functional theory (DFT) and wave function theory (WFT), we demonstrate that the global

Received: August 13, 2024
Revised: September 9, 2024
Accepted: September 11, 2024
Published: September 17, 2024

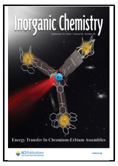

https://doi.org/10.1021/acs.inorgchem.4c03446

minimum structure of U_2B_6 is indeed an inverse sandwich. This structure features all four types of chemical bonds: σ, π, δ, and ϕ. Although the $\phi\cdots\phi$ bonding orbital, formed by two U 5f orbitals and three-node antibonding σ_{s3} group orbitals of B_6, is singly occupied, it still contributes non-negligibly (1.7%) to the total orbital interaction between U⋯U and B_6. Furthermore, the uranium diboride UB_2 solid phase, which can be viewed as "cluster-assembly materials"[34] comprising U_2B_6 units, also exhibits this ϕ bonding. This work provides theoretical insights into identifying $\phi\cdots\phi$ bonding in f-element compounds.

2. COMPUTATIONAL METHODS AND DETAILS

2.1. Global Minimum Search. The global minimum searches of U_2B_6 were carried out using a guaranteed escape strategy with supervised seed generation. In this method, seeds are generated based on point-group symmetry and covalent bonding distance criteria.[35] The energy of each seed is calculated using *ab initio* methods, and seeds are then sorted by energy. A geometry optimization is then performed on the top seeds, and these structures are then added to a stack. Until the stack is empty, each structure undergoes individual displacement of atomic Cartesian coordinates in both positive and negative directions. This process continues until an energy decrease is observed, indicating that the local minimum well has been successfully escaped. The optimized structure is then added to the stack. At each step, the structure is evaluated based on three criteria. The first ensures that no interatomic distance within the structure is shorter than the minimum threshold determined by covalent bonding radii data for each atom. The second criterion verifies that no atom has dissociated from the molecule. The third criterion ensures that the structure is unique relative to all previously evaluated structures. *Ab initio* calculations are not performed on any structure that fails any of the criteria. This method will be further detailed in an upcoming publication from our group.

2.2. Electronic Structure Determination. During the global minimum search, the energy of the structure is determined using GGA Perdew−Burke−Ernzerhof (PBE) density functional[36] with double-ζ plus one polarization (DZP)[37] slater type basis sets generated from the ADF 2023.102 program.[38,39] The relative energies of the 30 lowest-lying isomers were then recalculated with triple-ζ plus one polarization (TZP) basis set and examined using a hybrid PBE0 functional.[40] Different spin states (triplet, quintet, and septuplet) were considered during the search using spin-unrestricted calculations. It should be mentioned that the PBE functional has been reported in prior work to be a reliable method for the chemical bonding analyses of actinide compounds.[41−43] We carried out the scalar relativistic ZORA formalism[44] in order to account for the relativistic effect. The frozen core approximation was applied to B [$1s^2$] and [$1s^2$−$4f^{14}$] for the actinide elements. We further performed SO relativistic effect ZORA calculations to examine the bonding change influenced by the strong spin−orbit (SO) coupling effect for actinide elements.

Among the generated isomers, the D_{6h} ($^7A_{2g}$) inverse sandwich structure was identified as the global minimum using the PBE and PBE0 DFT methods. To achieve more accurate relative energies, we performed single-point DLPNO-UCCSD(T) open-shell calculations based on the unrestricted Hartree−Fock approach for the three lowest-lying isomers using the ORCA 5.0.4 package.[45,46] Herein, def2-TZVP basis sets were used for B,[47] utilizing the AutoAux generation procedure. For the U element, the small-core scalar relativistic effective core potential (SC-RECP) was employed in conjunction with the [10s9p5d4f3g] basis set.[48−50] Figure 1 displays the front and top views of the global minimum of U_2B_6, and the coordinates are listed in Table S1 in the Supporting Information. Alternative low-lying isomers within 50 kcal/mol at the levels of PBE and PBE0 combined with TZP basis sets are shown in Figure S1.

A complete-active-space self-consistent-field (CASSCF) calculation,[51] using the same basis sets and effective core potentials (ECPs) as implemented in ORCA 5.0.4, was performed to investigate the multireference character. Based on the selection methods for bonding and antibonding orbitals[52] in the active space for the actinide-containing compounds,[53,54] and inspired by the study of Ln_2B_8 lanthanide species (Ln = La, Pr),[33] we selected 20 orbitals with 10 electrons for the active space in this case. This chosen active space comprises six bonding orbitals, their corresponding six antibonding counterparts, and eight nonbonding 5f orbitals. Further details are provided in the Section 3.

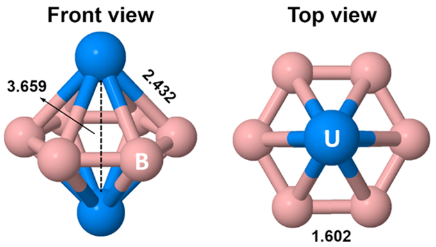

Figure 1. Front and top views of the neutral D_{6h} U_2B_6, where the structures are optimized at the PBE/TZP level. The bond lengths are in Å.

2.3. Chemical Bonding Analyses. In the bonding analysis of the B_6 ring, we used a right-handed local coordinate system (LCS) on each boron atom where the *z*-axis points to the center of the hexagon, with the *x*-axis lying in the plane and the *y*-axis perpendicular to the plane.[55] Energy decomposition analysis in conjunction with natural orbitals for chemical valence (EDA-NOCV) analysis[56−58] is an essential method to decompose the total interaction energy into different energy terms, which are electrostatic interaction, Pauli repulsion, and orbital interaction. It can also analyze the contributions of each orbital interaction to the total one, e.g., σ-, π-, δ-, and ϕ-bonding in this case. To figure out the multicenter bonding behavior of U_2B_6, we also carried out adaptive natural density partitioning (AdNDP) analyses.[59]

Crystal orbital Hamilton populations (COHP)[60] and the projected local combination of atomic orbitals (LCAO) wave function in the real space were calculated from the self-consistent PAW function by VASP 5.4.4 software,[61,62] as calculated by the LOBSTER package[63,64] and presented in the conventional manner:[65] we plotted −COHP (E) figure so that bonding contributions lie to the right and antibonding ones to the left. Fermi level was set to be zero in this work. We used a Γ-centered γ k grid of sizes of 9 × 9 × 6 and 18 × 18 × 13 for structural relaxation and static calculation, respectively. The cutoff energy of the plane-wave basis sets was set to 500 eV.

3. RESULTS AND DISCUSSION

3.1. Ground State and Electronic Structure of U_2B_6. As depicted in Figure S1, different spin states lead to distinct structural configurations with varying chemical bonding mechanisms. The results from both PBE0 and CCSD(T) methods indicate the predominant stability of the D_{6h} U_2B_6 ($^7A_{2g}$) inverse sandwich structure compared with other isomers. The second-lowest energy isomer **2** (C_s, $^5A''$) with a quintet spin state, referred to as the "quasi-borozene" structure,[66] is 15.56 kcal/mol higher at the CCSD(T) level than the global minimum. The T_1 diagnostic value of 0.03 for this isomer indicates a minimal multireference effect.[67] Similar to the La−La bonding observed in the La_2B_6 system,[66] this structure exhibits U−U bonding characterized by σ and π bonding patterns. Additionally, isomers **3** and **6** are also identified as inverse sandwich structures but are significantly higher in energy. The quintet isomer **3**, featuring triply occupied d−p−d δ bonding orbitals, undergoes a first-order Jahn−Teller distortion from D_{6h} to C_{2h}. The triplet isomer **6** exhibits a shorter U⋯U distance due to fully occupied $\delta\cdots\delta$ bonding orbitals. Isomer **12** exhibits a ribbon-like B_6 moiety

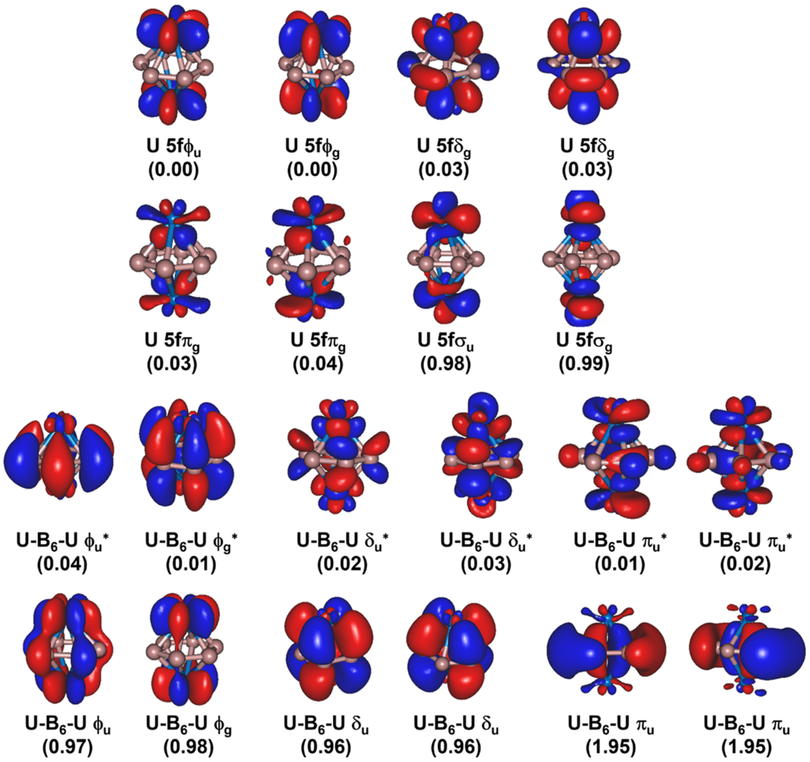

Figure 2. Natural orbital contours (isosurface value = 0.03 au) of U_2B_6 along with the corresponding occupation numbers from CASSCF (10e, 20o) calculations. The first two rows depict the nonbonding 5f orbitals of uranium, while the bottom two rows show the bonding orbitals and their antibonding counterparts, labeled with an asterisk (*).

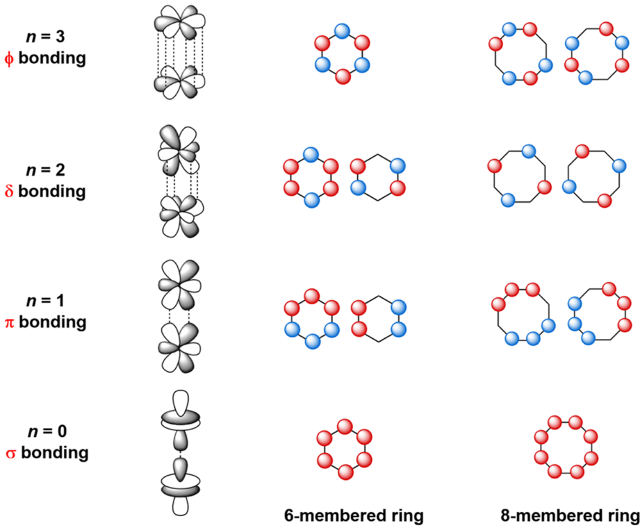

Figure 3. Schematic orbital contours for six and eight-membered boron/carbon rings with different number *n* of nodal planes, which could participate in σ, π, or δ and ϕ interactions with metal-based orbitals. Red and blue represent different orbital phases.

coordinating with two U atoms, where the B_6 structure resembles the global minimum structure of the bare B_6 cluster.[68] Notably, the bowl-like C_{5v} structure of B_6, which is another possible isomer of the B_6 cluster, coordinates with the two U atoms at significantly higher energy (>50 kcal/mol) compared to the global minimum isomer **1**.

The above single-configurational results are then examined using the CASSCF method in a multiconfigurational framework for the ground state of isomer **1**. Contours of Löwdin natural orbitals and the corresponding natural orbital occupation numbers obtained from the CASSCF (10e, 20o) method are depicted in Figure 2. As mentioned above, the selection method for the active space is based on the bonding, antibonding, and nonbonding characters for large systems.[53,54] We selected six U−B_6−U bonding orbitals, as depicted in the bottom row of Figure 2 (two π_u, two δ_u, one ϕ_g, and one ϕ_u), of which the six corresponding antibonding counterparts are shown in the second row from the bottom. The eight nonbonding 5f orbitals (one 5fϕ_u, one 5fϕ_g, two 5fδ_g, two 5fπ_g, one 5fσ_u, and one 5fσ_g) are illustrated in the first two rows. CASSCF results show that the ground state of the U_2B_6 complex is dominated by a single configuration of $[\cdots\pi^4\delta^2\phi^1\phi'^1U(5f\sigma)^1U(5f\sigma)^1]$ with a CI weight of 84%, indicating a subtle multireference character in this system, reinforcing the reliability of bonding descriptions at both the DFT and CCSD(T) levels. The effective bond order (EBO)[69] of U···B_6···U ϕ bonding interaction is calculated to be (0.97−0.04)/2 = 0.47. Comparably, the EBO of δ-bond from CASSCF (12e, 12o) calculation in $[Re_2Cl_8]^{2-}$ is reported to be 0.54,[70] further supporting the bonding effect of such ϕ bonding in U_2B_6.

3.2. Rationality of the Construction of the $\phi\cdots\phi$ Bonding. Next, we aimed to address the following question: why was U_2B_6 selected for the investigation of $\phi\cdots\phi$ bonding formation? As shown in Figure 3, we compared the reduced orbitals with different numbers of nodal planes for both six-membered and eight-membered rings to illustrate the formation of various types of chemical bonds. The colored orbitals in each row represent ligand group orbitals with different phases, which can potentially interact with metal orbitals of the same phase to form the corresponding bonding

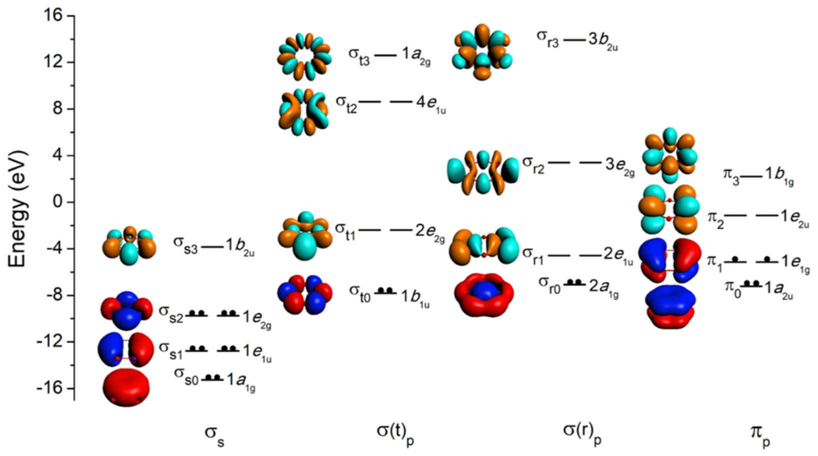

Figure 4. B_6 MOs in the local coordinate system (LCS) at the PBE0/TZP level. The valence MOs are divided into four subgroups: σ_s, $\sigma(t)_p$, $\sigma(r)_p$, and π_p. Herein, "t" and "r" denote "tangential" and "radial," respectively, with regard to the plane of B_6.

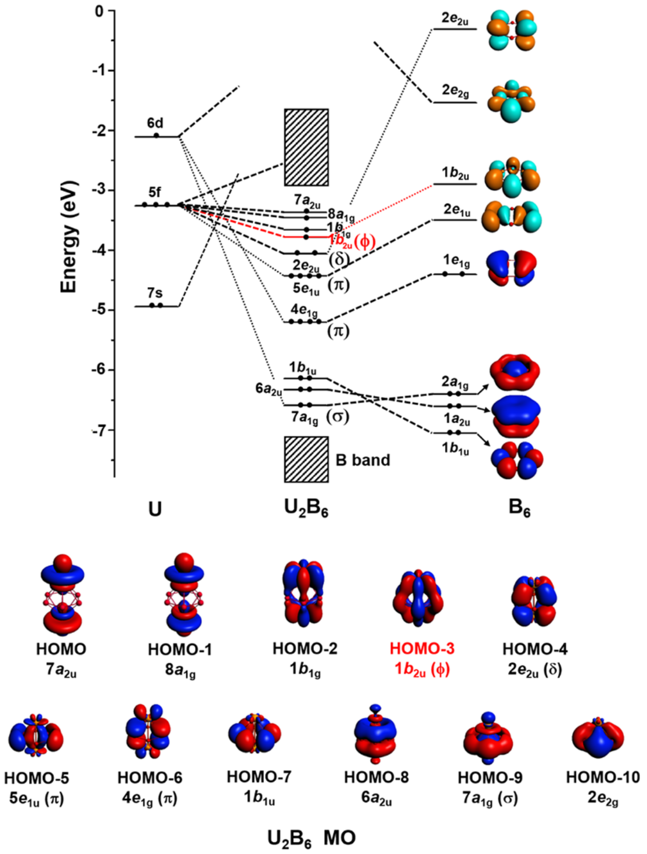

Figure 5. Orbital energy-level correlation diagram of U_2B_6 complex from U and B_6 fragments and the CMO contours (isovalue = 0.025 au) of U_2B_6. $1b_{2u}$ is highlighted in red to show the $\phi\cdots\phi$ bonding. HOMO − 9/5 ($7a_{1g}/5e_{1u}$), HOMO − 6 ($4e_{1g}$), and HOMO − 4 ($2e_{2u}$) correspond to σ, π, and δ-bonding, respectively.

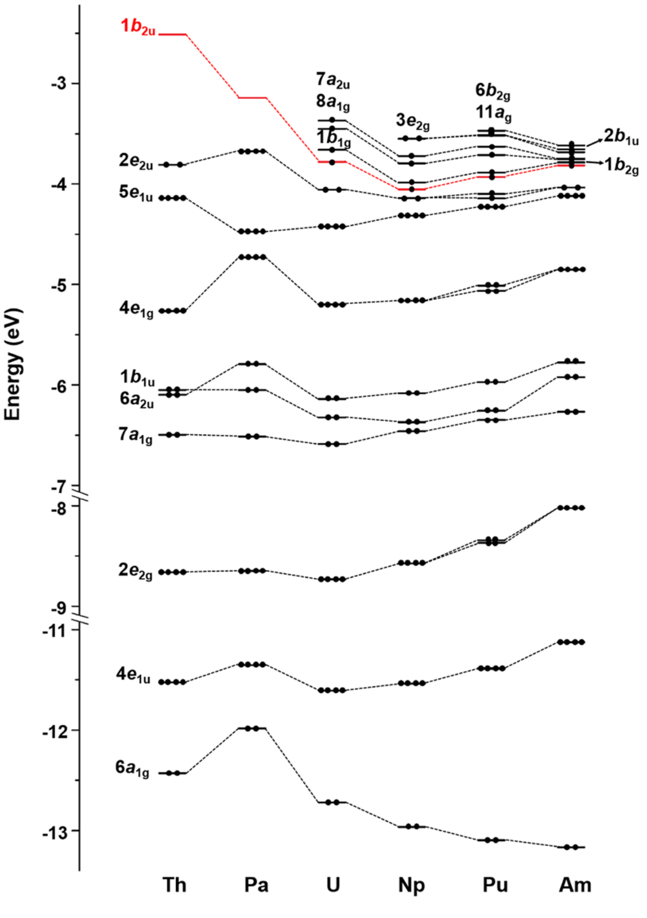

Figure 6. Energies of the frontier CMOs of the neutral An_2B_6 molecules (An = Th−Am) at the PBE/TZP level. $1b_{2u}$ highlighted in red corresponds to the ϕ-type bonding.

interactions. σ- and π-types of bonding interactions have been observed to dominate in inverse sandwich complexes.[71,72] δ character emerges when the central ring has a size $n \geq 6$, such as in the cases of uranium (*E*)-stilbene complexes[32] bridged by aromatic hydrocarbons, and lanthanide boron complexes[33] with two lanthanide atoms sandwiching a B_8 central ring. Importantly, orbitals of central ligands with three nodal planes, as shown in the first row of Figure 3, theoretically have the potential to form "face-to-face" $\phi\cdots\phi$ bonding with appropriate 4f/5f metals through suitable symmetry and efficient overlap, although this has not been extensively studied.

In order to interact with 5fϕ orbitals forming chemical bonds, the orbitals of the sandwiched ring are supposed to have comparable energy levels and be diffused enough over a large space to allow the effective overlap and preferable energy matching with 5fϕ orbitals.[27,73−77] As depicted in Figure S2, energy levels of the B_n ring lie higher than those of C_nH_n analogous due to the low electronegativity of boron. Therefore,

Table 1. EDA-NOCV Results for U_2B_6 at the PBE/TZP Level, Where $\Delta E_{int} = \Delta E_{Pauli} + \Delta E_{elstat} + \Delta E_{orb}$[a]

ΔE_{orb}			α			β	
Bonding Character	Energy Percent	$\Delta E_{orb}{}^{\alpha}$	$\Delta\rho_{\alpha}$	Orbital Contour	$\Delta E_{orb}{}^{\beta}$	$\Delta\rho_{\beta}$	Orbital Contour
$\Delta E_{orb}{}^{1}$ (π)	-764.2 (56.0%)	-183.9 × 2 (27.0%)	U_2 f$\pi \rightarrow B_6\ \sigma_{r1}$	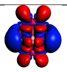	-198.2 × 2 (29.0%)	U_2 f$\pi \rightarrow B_6\ \sigma_{r1}$	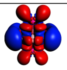
$\Delta E_{orb}{}^{2}$ (π)	-293.4 (21.5%)	-20.7 × 2 (3.0%)	U_2 d$\pi \leftarrow B_6\ \pi_1$	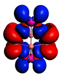	-126.0 × 2 (18.5%)	U_2 f$\pi \rightarrow B_6\ \pi_1$	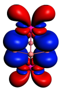
$\Delta E_{orb}{}^{3}$ (δ)	160.0 (11.7%)	-80.0 × 2 (11.7%)	U_2 d$\delta \rightarrow B_6\ \pi_2$	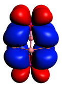			
$\Delta E_{orb}{}^{4}$ (σ)	-49.2 (3.6%)	-25.5 (1.9%)	U_2 (df)$\sigma \leftarrow B_6\ \sigma_{r0}$	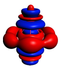	-23.7 (1.7%)	U_2 d$\sigma \rightarrow B_6\ \sigma_{r0}$	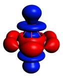
$\Delta E_{orb}{}^{5}$ (ϕ)	-23.2 (1.7%)	-23.2 (1.7%)	U_2 f$\phi \rightarrow B_6\ \sigma_{s3}$	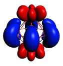			
ΔE_{orb}				-1324.56			
ΔE_{Pauli}				1947.93			
ΔE_{elstat}				-1118.32			
ΔE_{int}				-494.96			

[a] The major orbital components (ΔE^{i}_{orb}) of the total orbital interaction ΔE_{orb} are presented. Insert plots are the deformation densities $\Delta\rho$ (isosurface = 0.03 au) of the pairwise orbital interactions between U···U ($d\pi_u^4 d\delta_u^2 f\pi_g^2 f\phi_g^1 f\phi_u^1 f\sigma_g^1 f\sigma_u^1$) and B_6 ($\sigma_{r0}^2\pi_1^2\sigma_{r1}^0$) fragments and the associated interaction energies ΔE_{orb} (in kcal/mol). The value in parentheses gives the percentage contribution to the total orbital interaction ΔE_{orb}. The direction of the charge flow is from red to blue.

compared to the carbocyclic rings, boron rings are the more rational candidates to promote the formation of $\phi\cdots\phi$ bonding by means of tuning the antibonding orbital levels upon the different ring sizes of B_n and forming more diffused ligand group orbitals with the stronger 2s/2p hybridization than that of hydrocarbon analogous.[78−81]

To test the existence of $\phi\cdots\phi$ bonding facilitated by the boron ring, we first investigated the U_2B_8 system, inspired by the La_2B_8 inverse sandwich cluster.[33] The contours of the frontier orbitals of U_2B_8 are presented in Figure S3. However, no $\phi\cdots\phi$ bonding was observed due to the mismatch between the 5fϕ and σ_{s3} orbitals, as referenced in Figure 3 of ref 33. We then proceeded to investigate the U_2B_6 system by performing LCS analyses of the B_6 moiety at the PBE0/TZP level, as shown in Figure 4. Twenty-four molecular orbitals (MOs) formed with 2s and 2p atomic orbitals (AOs) are representatively divided into four groups: σ_s, $\sigma(t)_p$, $\sigma(r)_p$, and π_p, where "t" and "r" represent "tangential" and "radial," respectively. Subscripts of each orbital correspond to the number of the nodal planes. Consequently, in light of the orbital shape of U···U bonding and phase congruence with B_6 moiety, σ-, π-, and δ-types bonding are involved by the symmetry-adapted group orbitals of B_6 and the corresponding U···U 5f/6d σ-, π-, and δ-orbitals, respectively. Interestingly, benefiting from the appropriate size of the ring and the preferable energies, σ_{s3} of B_6 with three nodes can perfectly interact with 5fϕ_u orbitals of U···U to form an unprecedented $\phi\cdots\phi$ bonding to stabilize further the inverse sandwich U_2B_6 (details are provided in Section 3.3).

3.3. $\phi\cdots\phi$ Bonding in U_2B_6 Facilitated by the B_6 Ring.

Energy-level correlations and MOs of the global minimum structure of U_2B_6 are depicted in Figure 5, constructed from U and B_6 fragments. From the MO contours shown in the bottom part, we can visualize four different types of delocalized chemical bonds modulated by the central B_6 ring: σ ($7a_{1g}$), π ($4e_{1g}$, $5e_{1u}$), δ ($2e_{2u}$), and ϕ ($1b_{2u}$). AO compositions of each MO are shown in Table S2. Among the six unpaired electrons, two ($7a_{2u}$ and $8a_{1g}$) are the 5fσ electrons with little 6d and 7s hybridization, two come from the 5fϕ orbitals, and the rest two are corresponding to the singly occupied δ bonding. $1b_{2u}$, as highlighted in red in Figure 5, is the singly occupied $\phi\cdots\phi$ bonding resulting from the interactions between U···U 5fϕ_u and B_6 σ_{s3} group orbital (Figure 4), which is constituted by 80.5% U 5f, 16.4% B 2s, and 6.3% B 2p components. $1b_{1g}$ dominantly consisting of U_2 5fϕ_g (96.8%) with little contributions from B_6 2p σ_{r3} orbitals feature mainly nonbonding character. The partially occupied $1e_{1g}$ group orbital of the B_6 unit accepts two additional electrons from the U atoms, forming the $4e_{1g}$ MO in the U_2B_6 complex. Furthermore, four electrons from the U atoms are transferred to the originally unoccupied $2e_{1u}$ orbital of the B_6 moiety, resulting in the formation of $2e_{2u}$ with d−p−d δ bonding character. The remaining singly occupied orbitals can be considered dominated by the U 5f AOs. Consequently, the oxidation state (OS) of uranium in U_2B_6 is proposed to be +III. This is in contrast to the more common +IV OS observed in most uranium sandwich complexes,[82,83] a difference attributed to the low electronegativity of boron clusters. It is worth mentioning that isomer **6** with U (+IV) in Figure S1 lies 7.56 kcal/mol higher than the global minimum at the CCSD(T) level. Moreover, actinide compounds usually demonstrate a strong SO coupling effect,[43,84−86] which can influence the chemical bonding patterns.[87,88] Figure S4 illustrates the SO splitting of the scalar relativistic Kohn−Sham MO levels. The results indicate that despite the significant energy-level splitting in orbitals predominantly composed of uranium, the SO coupling

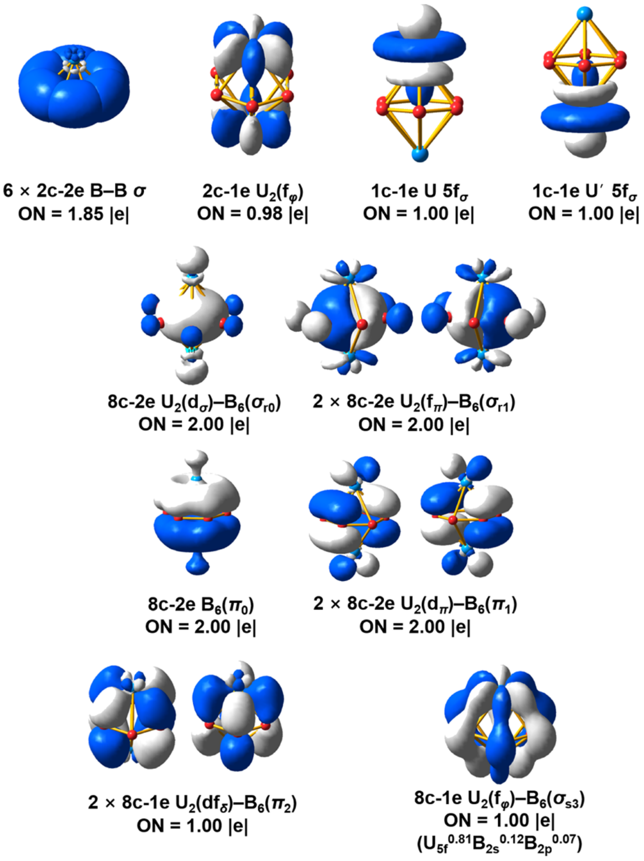

Figure 7. AdNDP bonding analyses of U_2B_6 at the PBE/TZP level. "ON" represents "occupation number" here. The AO composition of the multicenter $\phi\cdots\phi$ bonding is listed in parentheses.

effect does not significantly impact the understanding of the chemical bonding in U_2B_6.

We also examined other An_2B_6 (An = Th–Am) inverse sandwiches to search for similar $\phi\cdots\phi$ bonding with U_2B_6. Optimized Cartesian coordinates of each species are listed in Table S3. Correlation diagrams of energy levels and the corresponding orbital compositions are depicted in Figure 6 and Table S4, respectively. Unfortunately, $1b_{2u}$ orbitals with $\phi\cdots\phi$ bonding character in D_{6h} Th_2B_6 and Pa_2B_6 are virtual in their ground states due to the relatively higher energies of the 5fϕ orbitals compared to those in U_2B_6. In the later actinide complexes (Np_2B_6, Pu_2B_6, and Am_2B_6), $1b_{2u}$ is almost a 5fϕ nonbonding orbital (5f component >98%) because of the contraction of 5f shell in the later actinide elements. Thus, U_2B_6 is the unique species among the considered complexes, which possesses $\phi\cdots\phi$ bonding due to the effective overlap and energy matching between the 5fϕ_u orbital of U$\cdots$U and the σ_{s3} orbital of the B_6 ring.

Spin-unrestricted EDA-NOCV calculations are carried out to further obtain detailed insight into the interactions between the U$\cdots$U and B_6 fragments. Five major orbital components were found (ΔE_{orb}^1 − ΔE_{orb}^5), with the corresponding deformation densities ($\Delta\rho_1$ − $\Delta\rho_5$) presented in Table 1. Among them, the orbital term ΔE_{orb}^1 ($\pi\cdots\pi$ bonding) via U_2 5fπ and σ_{r1} orbitals of B_6 is the strongest orbital interaction, which provides 56.0% of the total orbital interactions ΔE_{orb}. The other π-type (ΔE_{orb}^2) bond formed by U_2 (5f/6d)π and π_1 orbitals of B_6 accounts for 21.5% of the total orbital interactions. Two singly occupied $\delta\cdots\delta$ bonding orbitals derived from 6dδ_u of U$\cdots$U and π_2 orbitals of B_6 contribute 11.7% in total, which is slightly smaller than that in the La_2B_8 inverse sandwich.[33] Remarkably, due to the favorable energy matching and symmetry compatibility between the 5fϕ_u orbital of U$\cdots$U and the σ_{s3} orbital of B_6, the corresponding contribution of ΔE_{orb}^5 is as high as 23.2 kcal/mol, accounting for 1.7% of the total orbital interaction. To provide a quantitative comparison, we also conducted EDA-NOCV analyses of the quadruple bond in $[Re_2Cl_8]^{2-}$, as summarized in Table S5. The δ-type bonding in $[Re_2Cl_8]^{2-}$ contributes only 0.8% (1.8 kcal/mol) to the total orbital interaction, consistent with the findings of Frenking et al.[89] Therefore, although the percentage contribution of the $\phi\cdots\phi$ bonding is relatively small, it remains a significant factor in the stability of the system and cannot be overlooked.

A clearer view of the chemical bonding classification of the U_2B_6 inverse sandwich is provided by AdNDP analyses[59] (Figure 7) in order to discuss the aromaticity and stability. Except for six B–B σ bonds and three 5f electrons in the first row, the rest of the multicenter bonds are mainly divided into four categories. σ_{r0} and σ_{r1} of B_6 can interact with U$\cdots$U 5dσ_g or 5fπ_u orbitals to form in-plane delocalized bonding. π_0 and π_1 orbitals of B_6 tend to participate in the bonding perpendicular to the plane with little U$\cdots$U 7s and 6dπ_g orbitals, respectively. The 12 delocalized electrons in rows 2 and 3 individually satisfy the $4n + 2$ Hückel rule, giving rise to the in-plane σ and π double aromaticities for the U_2B_6 inverse sandwich. Moreover, two degenerate singly occupied δ bonds are constructed from the π_2 orbital of B_6 moiety and 5d/6f δ_u orbital of U$\cdots$U. Thus, the valence electrons of U_2B_6 fulfill the "$2(x + 6 + y)$ rule" for the inverse sandwich complex, which was proposed by Li, Wang, and co-workers very recently,[25] where $x = 6$, $y = 1$, thus providing further evidence for the rather high chemical stability. Of particular importance is the delocalized ϕ-bonding primarily from B_6 σ_{s3} and U$\cdots$U 5fϕ_u orbitals, where the composition of U 5f is calculated to be 81%.

3.4. U_2B_6 as the Building Unit for UB_2 Solid.

Employing a similar self-assembly method used in the study of the La_2B_8 cluster vs LaB_6 solid,[90] and the Mo_3S_4 cluster vs MoS_2 solid,[34] we compared the An_2B_6 cluster and the AnB_2 solid material (An = U, Np, Pu) in terms of geometric parameters, charge distribution,[91] and bonding characteristics, as shown in Table S6. For simplicity, we only discussed the uranium case as an example. From the high resemblance between the two cases, the UB_2 periodic system can be considered as the two-dimensional expansion from the U_2B_6 building block (Figure 8a). Although the An–B and B–B distances in the UB_2 system are slightly shorter than those in the molecular systems, the B–B bonding strength is stronger, consistent with previous studies comparing the Ln_2B_8 and LnB_6 systems.[90]

According to the density of states (DOS) shown in Figure 8b, the hybridization between 5f and 6d components is stronger in the U_2B_6 case, indicating that covalency plays a larger role in isolated U_2B_6 compared to the UB_2 solid state.[90] Further insights into the chemical bonding comparison of the B–B and U–B interactions in both the U_2B_6 and UB_2 systems are provided in Figure 8c and Table S6, both of which demonstrate that the overall bonding patterns between the cluster and solid systems are similar. Below the Fermi level (occupied region) in both systems, the interactions predominantly arise from bonding states without antibonding contributions in the valence band, indicating high stabilities.

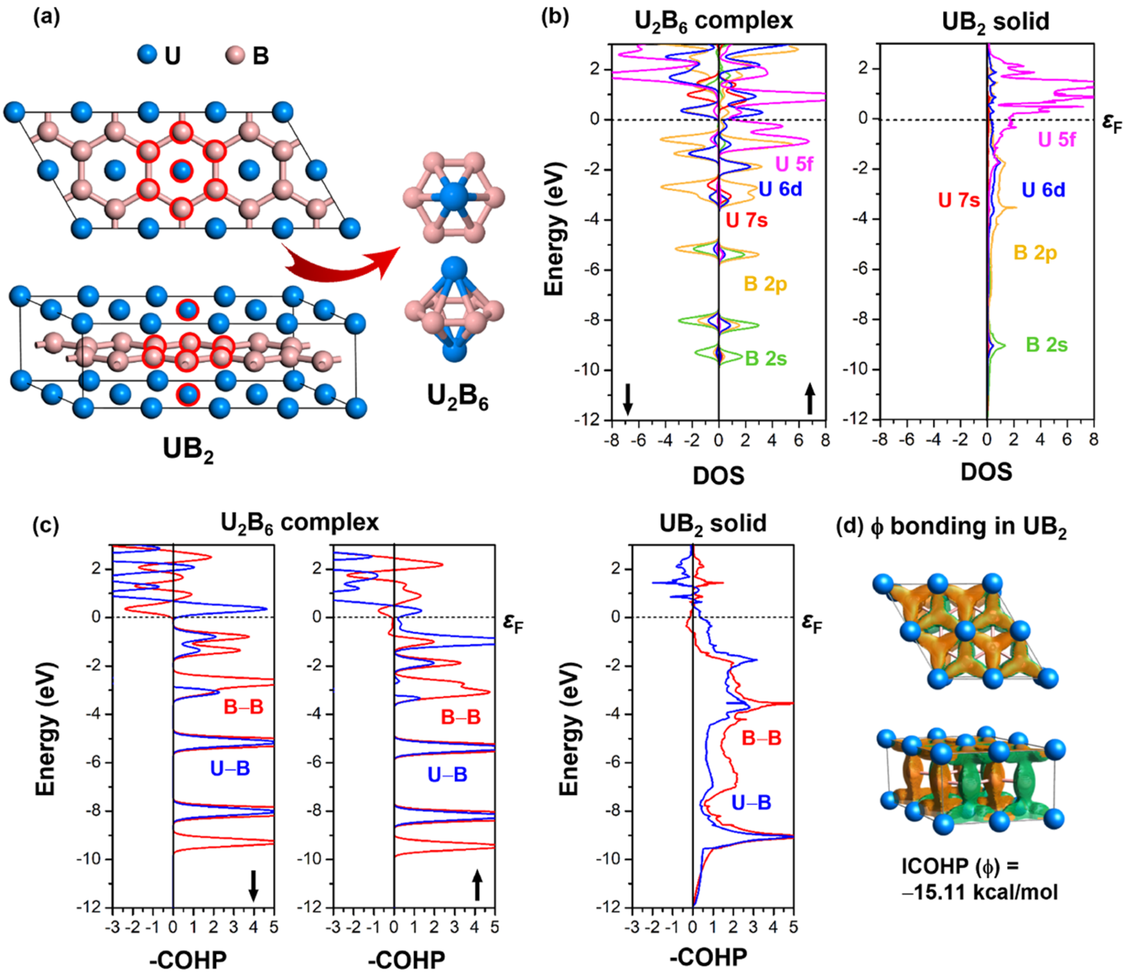

Figure 8. (a) Top and side views of UB_2 hexagonal crystalline structure, with the U_2B_6 unit highlighted in red. (b) pDOS figures of both the U_2B_6 complex and the UB_2 crystal. (c) COHP analyses of U−B and B−B interactions of the U_2B_6 complex and the UB_2 crystal. (d) ϕ bonding of the UB_2 crystal with the corresponding ICOHP value. Here, Fermi levels of all of the plots were shifted to zero for better comparison.

An energy integration up to the Fermi level (ICOHP) can be used to compare the strengths of each orbital-pair interaction. In Figure 8d, we show the result of ϕ bonding contour projected on the Γ-point in the real space of the UB_2 crystal, along with the corresponding ICOHP value. Other types of bonding, such as σ, π, and δ, are detailed in Figure S5, indicating that the B_6 ring acts as a unit that enhances the interaction between the B and U atoms on the upper and lower sheets. An obvious bonding peak of 5fϕ character was found, most pronounced in the area approximately 1 eV below the Fermi level, contributing 3.8% (−15.11 kcal/mol) to the total bonding in a unit cell, which agrees well with the MO diagram in Figure 5. The dominant bonding character of the U−B interaction in the UB_2 solid originates from π bonding, with an ICOHP value as large as −232.45 kcal/mol (58.5%) in a unit cell.

4. CONCLUSIONS

Over the past hundred years, the concept of chemical bonds has emerged as an exciting area in the modern chemistry field. Different covalent interactions such as σ-, π-, and δ-types of bonding patterns have been extensively studied, especially in compounds with multiple bonds. Our theoretical analyses have shown that the global minimum of U_2B_6 has D_{6h} symmetry with six unpaired electrons, presenting σ-, π-, δ-, and ϕ-types of bonding character. A singly occupied $\phi\cdots\phi$ bonding orbital was found with the contribution of 1.7% to the total orbital interaction, involving the U 5fϕ and the three-node in-plane group orbital of the B_6 ring. The comparison between the U_2B_6 complex and UB_2 solid suggests various similarities between these two systems regarding geometry, electronic structure, and chemical bonding. The non-negligible ϕ bonding is also found in UB_2 solid, contributing to the chemical bonding. Thus, the study of cluster science can help us to better understand the stability of solid-state materials. Overall, the current results have enriched the categories of chemical bonding and provided theoretical evidence for the potential feasibility of the diactinide-boron inverse sandwich complexes. In principle, other types of chemical bonding with higher quantum number of orbital angular momentum are not impossible, e.g., $L = \pm 4$ (γ), ± 5 (η), ± 6 (I), ⋯, while it still remains a challenge due to the scarcity of the known chemical elements containing ng-orbitals and the rather weak overlap between the higher valence shell orbitals.

■ ASSOCIATED CONTENT

Supporting Information

The Supporting Information is available free of charge at https://pubs.acs.org/doi/10.1021/acs.inorgchem.4c03446.

Cartesian coordinates of D_{6h} An_2B_6 species; AO contributions to the frontier orbitals; EDA-NOCV analyses of $[Re_2Cl_8]^{2-}$; a comparison between AnB_2 and An_2B_6; a list of possible isomers within 50 kcal/mol; a comparison between B_n and C_nH_n analogous; frontier orbitals of U_2B_8; relativistic effect; and chemical bonding pattern of UB_2 solid (PDF)

■ AUTHOR INFORMATION

Corresponding Author

Wan-Lu Li – *Aiiso Yufeng Li Family Department of Chemical and Nano Engineering, University of California, San Diego, La Jolla, California 92093, United States; Program of Materials Science and Engineering, University of California, San Diego, La Jolla, California 92093, United States;* orcid.org/0000-0003-0098-0670; Email: wal019@ucsd.edu

Author

Jordan Burkhardt – *Aiiso Yufeng Li Family Department of Chemical and Nano Engineering, University of California, San Diego, La Jolla, California 92093, United States; Department of Chemistry and Biochemistry, University of California, San Diego, La Jolla, California 92093, United States*

Complete contact information is available at:
https://pubs.acs.org/10.1021/acs.inorgchem.4c03446

Notes

The authors declare no competing financial interest.

■ ACKNOWLEDGMENTS

The calculations were performed using Expanse supercomputer at the San Diego Supercomputer Center (SDSC), through allocations of CHM230035, CHM240026, and CHE230113. W.-L.L. acknowledges start-up funding from the Jacobs School of Engineering, UCSD.

■ REFERENCES

(1) Pauling, L. The nature of the chemical bond. IV. The energy of single bonds and the relative electronegativity of atoms. *J. Am. Chem. Soc.* **1932**, *54*, 3570–3582.

(2) Pauling, L. *The Nature of the Chemical Bond and the Structure of Molecules and Crystals: An Introduction to Modern Structural Chemistry*, 3rd ed.; Cornell University Press, 1960.

(3) Ruedenberg, K. The Physical Nature of the Chemical Bond. *Rev. Mod. Phys.* **1962**, *34*, 326–376.

(4) Mulliken, R. S. Bonding Power of Electrons and Theory of Valence. *Chem. Rev.* **1931**, *9*, 347–388.

(5) Urey, H. C. The structure of atoms with particular reference to valence. *J. Chem. Educ.* **1931**, *8*, 1114.

(6) Mulliken, R. S. Chemical bonding. *Annu. Rev. Phys. Chem.* **1978**, *29*, 1–31.

(7) Kutzelnigg, W. Chemical bonding in higher main group elements. *Angew. Chem., Int. Ed.* **1984**, *23*, 272–295.

(8) Moore, J.; Stanitski, C.; Jurs, P. *Principles of Chemistry: The Molecular Science*; Cengage Learning, 2009.

(9) Cotton, F. A.; Murillo, C. A.; Walton, R. A. *Multiple Bonds between Metal Atoms*; Springer Science & Business Media, 2005.

(10) Power, P. P. π-Bonding and the Lone Pair Effect in Multiple Bonds between Heavier Main Group Elements. *Chem. Rev.* **1999**, *99*, 3463–3503.

(11) Cundari, T. R. Computational studies of transition metal-main group multiple bonding. *Chem. Rev.* **2000**, *100*, 807–818.

(12) Nguyen, T.; Sutton, A. D.; Brynda, M.; Fettinger, J. C.; Long, G. J.; Power, P. P. Synthesis of a stable compound with fivefold bonding between two chromium (I) centers. *Science* **2005**, *310*, 844–847.

(13) Tsai, Y.-C.; Chen, H.-Z.; Chang, C.-C.; Yu, J.-S. K.; Lee, G.-H.; Wang, Y.; Kuo, T.-S. Journey from Mo-Mo quadruple bonds to quintuple bonds. *J. Am. Chem. Soc.* **2009**, *131*, 12534–12535.

(14) Bursten, B. E.; Cotton, F. A.; Hall, M. B. Dimolybdenum: nature of the sextuple bond. *J. Am. Chem. Soc.* **1980**, *102*, 6348–6349.

(15) Cotton, F. A. Metal-metal bonding in $[Re_2X_8]^{2-}$ ions and other metal atom clusters. *Inorg. Chem.* **1965**, *4*, 334–336.

(16) Bursten, B. E.; Ozin, G. A. Xα-SW calculations for naked actinide dimers: existence of ϕ bonds between metal atoms. *Inorg. Chem.* **1984**, *23*, 2910–2911.

(17) Gagliardi, L.; Roos, B. O. Quantum chemical calculations show that the uranium molecule U_2 has a quintuple bond. *Nature* **2005**, *433*, 848–851.

(18) Pagano, J. K.; Xie, J.; Erickson, K. A.; Cope, S. K.; Scott, B. L.; Wu, R.; Waterman, R.; Morris, D. E.; Yang, P.; Gagliardi, L.; Kiplinger, J. L. Actinide 2-metallabiphenylenes that satisfy Hückel's rule. *Nature* **2020**, *578*, 563–567.

(19) Kelley, M. P.; Popov, I. A.; Jung, J.; Batista, E. R.; Yang, P. δ and φ back-donation in AnIV metallacycles. *Nat. Commun.* **2020**, *11*, No. 1558.

(20) Minasian, S. G.; Keith, J. M.; Batista, E. R.; Boland, K. S.; Clark, D. L.; Kozimor, S. A.; Martin, R. L.; Shuh, D. K.; Tyliszczak, T. New evidence for 5f covalency in actinocenes determined from carbon K-edge XAS and electronic structure theory. *Chem. Sci.* **2014**, *5*, 351–359.

(21) Popov, I. A.; Billow, B. S.; Carpenter, S. H.; Batista, E. R.; Boncella, J. M.; Tondreau, A. M.; Yang, P. An Allyl Uranium (IV) Sandwich Complex: Are ϕ Bonding Interactions Possible? *Chem.—Eur. J.* **2022**, *28*, No. e202200114.

(22) Li, W.-L.; Chen, T.-T.; Jiang, Z.-Y.; Wang, L.-S.; Li, J. Recent progresses in the investigation of rare-earth boron inverse sandwich clusters. *Jiegou Huaxue* **2020**, *39*, 1009–1018.

(23) Lu, X.-Q.; Chen, Q.; Tian, X.-X.; Mu, Y.-W.; Lu, H.-G.; Li, S.-D. Predicting lanthanide boride inverse sandwich tubular molecular rotors with the smallest core–shell structure. *Nanoscale* **2019**, *11*, 21311–21316.

(24) Chen, T.-T.; Li, W.-L.; Li, J.; Wang, L.-S. $[La(\eta_x\text{-}B_x)La]^-$ (x = 7–9): a new class of inverse sandwich complexes. *Chem. Sci.* **2019**, *10*, 2534–2542.

(25) Chen, T.-T.; Li, W.-L.; Chen, W.-J.; Li, J.; Wang, L.-S. $La_3B_{14}^-$: an inverse triple-decker lanthanide boron cluster. *Chem. Commun.* **2019**, *55*, 7864–7867.

(26) Liddle, S. T. Inverted sandwich arene complexes of uranium. *Coord. Chem. Rev.* **2015**, *293–294*, 211–227.

(27) Huang, W.; Diaconescu, P. L. Rare-earth metal Π-complexes of reduced arenes, alkenes, and alkynes: bonding, electronic structure, and comparison with actinides and other electropositive metals. *Dalton Trans.* **2015**, *44*, 15360–15371.

(28) Patel, D.; Tuna, F.; McInnes, E. J. L.; McMaster, J.; Lewis, W.; Blake, A. J.; Liddle, S. T. A triamido-uranium(V) inverse-sandwich 10Π-toluene tetraanion arene complex. *Dalton Trans.* **2013**, *42*, 5224–5227.

(29) Xiao, Y.; Zhao, X.-K.; Wu, T.; Miller, J. T.; Hu, H.-S.; Li, J.; Huang, W.; Diaconescu, P. L. Distinct electronic structures and bonding interactions in inverse-sandwich samarium and ytterbium biphenyl complexes. *Chem. Sci.* **2021**, *12*, 227–238.

(30) Deng, C.; Xu, X.-C.; Sun, R.; Wang, Y.; Wang, B.-W.; Hu, H.-S.; Huang, W. Topology-Dependent Synthesis, Structures, and Bonding Interactions of Uranium Polyarene Complexes. *Organometallics* **2024**, *43*, 174–190.

(31) Diaconescu, P. L.; Cummins, C. C. Diuranium inverted sandwiches involving naphthalene and cyclooctatetraene. *J. Am. Chem. Soc.* **2002**, *124*, 7660–7661.

(32) Diaconescu, P. L.; Cummins, C. C. μ-η^6, η^6-arene-bridged diuranium hexakisketimide complexes isolable in two states of charge. *Inorg. Chem.* **2012**, *51*, 2902−2916.

(33) Li, W.-L.; Chen, T.-T.; Xing, D.-H.; Chen, X.; Li, J.; Wang, L.-S. Observation of highly stable and symmetric lanthanide octa-boron inverse sandwich complexes. *Proc. Natl. Acad. Sci. U.S.A.* **2018**, *115*, E6972−E6977.

(34) Wang, B.; Li, W.-L. Revisiting the quasi-aromaticity in polynuclear metal chalcogenide clusters and their derivative "cluster-assembly" crystalline structures. *Phys. Chem. Chem. Phys.* **2024**, *26*, 17370−17382.

(35) Pyykkö, P.; Atsumi, M. Molecular Single-Bond Covalent Radii for Elements 1−118. *Chem.—Eur. J.* **2009**, *15*, 186−197.

(36) Perdew, J. P.; Burke, K.; Ernzerhof, M. Generalized Gradient Approximation Made Simple. *Phys. Rev. Lett.* **1996**, *77*, 3865−3868.

(37) Van Lenthe, E.; Baerends, E. J. Optimized Slater-type basis sets for the elements 1−118. *J. Comput. Chem.* **2003**, *24*, 1142−1156.

(38) *ADF 2024.1, SCM*; Vrije Universiteit: Amsterdam, The Netherlands, 2024. http://www.scm.com.

(39) te Velde, G.; Bickelhaupt, F. M.; Baerends, E. J.; Fonseca Guerra, C.; van Gisbergen, S. J. A.; Snijders, J. G.; Ziegler, T. Chemistry with ADF. *J. Comput. Chem.* **2001**, *22*, 931−967.

(40) Adamo, C.; Barone, V. Toward reliable density functional methods without adjustable parameters: The PBE0 model. *J. Chem. Phys.* **1999**, *110*, 6158−6170.

(41) Su, J.; Dau, P. D.; Qiu, Y.-H.; Liu, H.-T.; Xu, C.-F.; Huang, D.-L.; Wang, L.-S.; Li, J. Probing the Electronic Structure and Chemical Bonding in Tricoordinate Uranyl Complexes $UO_2X_3^-$ (X = F, Cl, Br, I): Competition between Coulomb Repulsion and U−X Bonding. *Inorg. Chem.* **2013**, *52*, 6617−6626.

(42) Chi, C.; Wang, J.-Q.; Qu, H.; Li, W.-L.; Meng, L.; Luo, M.; Li, J.; Zhou, M. Preparation and Characterization of Uranium−Iron Triple-Bonded $UFe(CO)_3^-$ and $OUFe(CO)_3^-$ Complexes. *Angew. Chem., Int. Ed.* **2017**, *56*, 6932−6936.

(43) Li, W.-L.; Burkhardt, J. AnB_8^-: borozene complexes with monovalent actinide. *Phys. Chem. Chem. Phys.* **2024**, *26*, 16091−16095.

(44) Lenthe, E. v.; Baerends, E. J.; Snijders, J. G. Relativistic regular two-component Hamiltonians. *J. Chem. Phys.* **1993**, *99*, 4597−4610.

(45) Neese, F. The ORCA program system. *Wiley Interdiscip. Rev.: Comput. Mol. Sci.* **2012**, *2*, 73−78.

(46) Guo, Y.; Riplinger, C.; Becker, U.; Liakos, D. G.; Minenkov, Y.; Cavallo, L.; Neese, F. Communication: An improved linear scaling perturbative triples correction for the domain based local pair-natural orbital based singles and doubles coupled cluster method [DLPNO-CCSD(T)]. *J. Chem. Phys.* **2018**, *148*, No. 011101.

(47) Weigend, F.; Ahlrichs, R. Balanced basis sets of split valence, triple zeta valence and quadruple zeta valence quality for H to Rn: Design and assessment of accuracy. *Phys. Chem. Chem. Phys.* **2005**, *7*, 3297−3305.

(48) Küchle, W.; Dolg, M.; Stoll, H.; Preuss, H. Energy-adjusted pseudopotentials for the actinides. Parameter sets and test calculations for thorium and thorium monoxide. *J. Chem. Phys.* **1994**, *100*, 7535−7542.

(49) Cao, X.; Dolg, M.; Stoll, H. Valence basis sets for relativistic energy-consistent small-core actinide pseudopotentials. *J. Chem. Phys.* **2003**, *118*, 487−496.

(50) Cao, X.; Dolg, M. Segmented contraction scheme for small-core actinide pseudopotential basis sets. *J. Mol. Struct.: THEOCHEM* **2004**, *673*, 203−209.

(51) Roos, B. O. The complete active space self-consistent field method and its applications in electronic structure calculations. *Adv. Chem. Phys.* **1987**, *69*, 399−445.

(52) Angeli, C.; Calzado, C. J.; Cimiraglia, R.; Evangelisti, S.; Mayna, D. Multiple complete active space self-consistent field solutions. *Mol. Phys.* **2003**, *101*, 1937−1944.

(53) Atkinson, B. E.; Hu, H.-S.; Kaltsoyannis, N. Post Hartree−Fock calculations of pnictogen−uranium bonding in EUF_3 (E = N−Bi). *Chem. Commun.* **2018**, *54*, 11100−11103.

(54) Wei, F.; Wu, G.; Schwarz, W.; Li, J. Geometries, electronic structures, and excited states of UN_2, NUO^+, and UO_2^{2+}: a combined CCSD(T), RAS/CASPT2 and TDDFT study. *Theor. Chem. Acc.* **2011**, *129*, 467−481.

(55) Li, W.-L.; Xu, C.-Q.; Hu, S.-X.; Li, J. Theoretical studies on the bonding and electron structures of a $[Au_3Sb_3]^{3-}$ complex and its oligomers. *Dalton Trans.* **2016**, *45*, 11657−11667.

(56) Ziegler, T.; Rauk, A. A theoretical study of the ethylene-metal bond in complexes between copper(1+), silver(1+), gold(1+), platinum(0) or platinum(2+) and ethylene, based on the Hartree-Fock-Slater transition-state method. *Inorg. Chem.* **1979**, *18*, 1558−1565.

(57) Michalak, A.; Mitoraj, M.; Ziegler, T. Bond Orbitals from Chemical Valence Theory. *J. Phys. Chem. A* **2008**, *112*, 1933−1939.

(58) Mitoraj, M. P.; Michalak, A.; Ziegler, T. A Combined Charge and Energy Decomposition Scheme for Bond Analysis. *J. Chem. Theory Comput.* **2009**, *5*, 962−975.

(59) Zubarev, D. Y.; Boldyrev, A. I. Developing paradigms of chemical bonding: adaptive natural density partitioning. *Phys. Chem. Chem. Phys.* **2008**, *10*, 5207−5217.

(60) Dronskowski, R.; Bloechl, P. E. Crystal orbital Hamilton populations (COHP): energy-resolved visualization of chemical bonding in solids based on density-functional calculations. *J. Phys. Chem. A* **1993**, *97*, 8617−8624.

(61) Kresse, G.; Furthmüller, J. Efficiency of ab-initio total energy calculations for metals and semiconductors using a plane-wave basis set. *Comput. Mater. Sci.* **1996**, *6*, 15−50.

(62) Kresse, G.; Furthmüller, J. Efficient iterative schemes for ab initio total-energy calculations using a plane-wave basis set. *Phys. Rev. B* **1996**, *54*, 11169−11186.

(63) Maintz, S.; Deringer, V. L.; Tchougréeff, A. L.; Dronskowski, R. Analytic projection from plane-wave and PAW wavefunctions and application to chemical-bonding analysis in solids. *J. Comput. Chem.* **2013**, *34*, 2557−2567.

(64) Maintz, S.; Deringer, V. L.; Tchougréeff, A. L.; Dronskowski, R. LOBSTER: A tool to extract chemical bonding from plane-wave based DFT. *J. Comput. Chem.* **2016**, *37*, 1030−1035.

(65) Dronskowski, R. *Computational Chemistry of Solid State Materials: A Guide for Materials Scientists, Chemists, Physicists and Others*; John Wiley & Sons, 2008.

(66) Burkhardt, J.; Chen, T.-T.; Chen, W.-J.; Yuan, D.-F.; Li, W.-L.; Wang, L.-S. Probing the Structures and Lanthanum−Lanthanum Bonding in $La_2B_n^-$ (n = 4−6) Clusters. *Inorg. Chem.* **2024**, *63* (37), 17215−17224.

(67) Li, W.-L.; Jian, T.; Chen, X.; Chen, T.-T.; Lopez, G. V.; Li, J.; Wang, L.-S. The Planar CoB_{18}^- Cluster as a Motif for Metallo-Borophenes. *Angew. Chem., Int. Ed.* **2016**, *55*, 7358−7363.

(68) Alexandrova, A. N.; Boldyrev, A. I.; Zhai, H.-J.; Wang, L.-S.; Steiner, E.; Fowler, P. W. Structure and Bonding in B_6^- and B_6: Planarity and Antiaromaticity. *J. Phys. Chem. A* **2003**, *107*, 1359−1369.

(69) Roos, B. O.; Borin, A. C.; Gagliardi, L. Reaching the maximum multiplicity of the covalent chemical bond. *Angew. Chem., Int. Ed.* **2007**, *46*, 1469.

(70) Gagliardi, L.; Roos, B. O. The electronic spectrum of $Re_2Cl_8^{2-}$: A theoretical study. *Inorg. Chem.* **2003**, *42*, 1599−1603.

(71) Evans, W. J.; Ulibarri, T. A.; Ziller, J. W. Reactivity of $(C_5Me_5)_2Sm$ with aryl-substituted alkenes: synthesis and structure of a bimetallic styrene complex that contains an η^2-arene lanthanide interaction. *J. Am. Chem. Soc.* **1990**, *112*, 219−223.

(72) Huang, W.; Abukhalil, P. M.; Khan, S. I.; Diaconescu, P. L. Group 3 metal stilbene complexes: synthesis, reactivity, and electronic structure studies. *Chem. Commun.* **2014**, *50*, 5221−5223.

(73) Street, K., Jr.; Seaborg, G. T. The separation of americium and curium from the rare earth elements. *J. Am. Chem. Soc.* **1950**, *72*, 2790−2792.

(74) Diamond, R. M.; Street, K. J.; Seaborg, G. T. An Ion-exchange Study of Possible Hybridized 5f Bonding in the Actinides1. *J. Am. Chem. Soc.* **1954**, *76*, 1461−1469.

(75) Seaman, L. A.; Wu, G.; Edelstein, N.; Lukens, W. W.; Magnani, N.; Hayton, T. W. Probing the 5f orbital contribution to the bonding in a U (V) ketimide complex. *J. Am. Chem. Soc.* **2012**, *134*, 4931−4940.

(76) Cross, J. N.; Su, J.; Batista, E. R.; Cary, S. K.; Evans, W. J.; Kozimor, S. A.; Mocko, V.; Scott, B. L.; Stein, B. W.; Windorff, C. J.; Yang, P. Covalency in Americium(III) Hexachloride. *J. Am. Chem. Soc.* **2017**, *139*, 8667−8677.

(77) Kelley, M. P.; Su, J.; Urban, M.; Luckey, M.; Batista, E. R.; Yang, P.; Shafer, J. C. On the origin of covalent bonding in heavy actinides. *J. Am. Chem. Soc.* **2017**, *139*, 9901−9908.

(78) Alexandrova, A. N.; Boldyrev, A. I.; Zhai, H.-J.; Wang, L.-S. All-boron aromatic clusters as potential new inorganic ligands and building blocks in chemistry. *Coord. Chem. Rev.* **2006**, *250*, 2811−2866.

(79) Sergeeva, A. P.; Popov, I. A.; Piazza, Z. A.; Li, W.-L.; Romanescu, C.; Wang, L.-S.; Boldyrev, A. I. Understanding boron through size-selected clusters: structure, chemical bonding, and fluxionality. *Acc. Chem. Res.* **2014**, *47*, 1349−1358.

(80) Wang, L.-S. Photoelectron spectroscopy of size-selected boron clusters: from planar structures to borophenes and borospherenes. *Int. Rev. Phys. Chem.* **2016**, *35*, 69−142.

(81) Li, W.-L.; Chen, X.; Jian, T.; Chen, T.-T.; Li, J.; Wang, L.-S. From planar boron clusters to borophenes and metalloborophenes. *Nat. Rev. Chem.* **2017**, *1*, No. 0071.

(82) Li, J.; Bursten, B. E. Bis(arene) Actinide Sandwich Complexes, $(\eta^6\text{-}C_6H_3R_3)_2An$: Linear or bent? *J. Am. Chem. Soc.* **1999**, *121*, 10243−10244.

(83) Li, J.; Bursten, B. E. Electronic structure of cycloheptatrienyl sandwich compounds of actinides: An $(\eta_7\text{-}C_7H_7)_2$ (An= Th, Pa, U, Np, Pu, Am). *J. Am. Chem. Soc.* **1997**, *119*, 9021−9032.

(84) Su, J.; Li, W.-L.; Lopez, G. V.; Jian, T.; Cao, G.-J.; Li, W.-L.; Schwarz, W. H. E.; Wang, L.-S.; Li, J. Probing the Electronic Structure and Chemical Bonding of Mono-Uranium Oxides with Different Oxidation States: UO_x^- and UO_x (x = 3−5). *J. Phys. Chem. A* **2016**, *120*, 1084−1096.

(85) Li, W.-L.; Su, J.; Jian, T.; Lopez, G. V.; Hu, H.-S.; Cao, G.-J.; Li, J.; Wang, L.-S. Strong electron correlation in UO_2^-: A photoelectron spectroscopy and relativistic quantum chemistry study. *J. Chem. Phys.* **2014**, *140*, No. 094306.

(86) Wei, F.; Wu, G.-S.; Schwarz, W. H. E.; Li, J. Excited States and Absorption Spectra of UF_6: A RASPT2 Theoretical Study with Spin−Orbit Coupling. *J. Chem. Theory Comput.* **2011**, *7*, 3223−3231.

(87) Wang, Y.-L.; Hu, H.-S.; Li, W.-L.; Wei, F.; Li, J. Relativistic Effects Break Periodicity in Group 6 Diatomic Molecules. *J. Am. Chem. Soc.* **2016**, *138*, 1126−1129.

(88) Li, W.-L.; Lu, J.-B.; Wang, Z.-L.; Hu, H.-S.; Li, J. Relativity−Induced Bonding Pattern Change in Coinage Metal Dimers M_2 (M = Cu, Ag, Au, Rg). *Inorg. Chem.* **2018**, *57*, 5499−5506.

(89) Krapp, A.; Lein, M.; Frenking, G. The strength of the σ-, π-and δ-bonds in $Re_2Cl_2^{2-}$. *Theor. Chem. Acc.* **2008**, *120*, 313−320.

(90) Li, W.-L.; Ertural, C.; Bogdanovski, D.; Li, J.; Dronskowski, R. Chemical Bonding of Crystalline LnB_6 (Ln = La−Lu) and Its Relationship with Ln_2B_8 Gas-Phase Complexes. *Inorg. Chem.* **2018**, *57*, 12999−13008.

(91) Mulliken, R. S. Electronic Population Analysis on LCAO−MO Molecular Wave Functions. I. *J. Chem. Phys.* **1955**, *23*, 1833−1840.